BULLETIN OF THE POLISH ACADEMY OF SCIENCES
TECHNICAL SCIENCES, Vol. 70(2), 2022, Article number: e140687
DOI: 10.24425/bpasts.2022.140687

Dynamic performance and stability analysis of an active inerter-based suspension with time-delayed acceleration feedback control

Yong WANG [1,2,3]*, Xian-Yu JIN [1], Yun-Shun ZHANG [1], Hu DING [4], and Li-Qun CHEN [4]

[1] Automotive Engineering Research Institute, Jiangsu University, Zhenjiang 212013, China
[2] Vehicle Measurement, Control and Safety Key Laboratory of Sichuan Province, Xihua University, Chengdu 610039, China
[3] Provincial Engineering Research Center for New Energy Vehicle Intelligent Control and Simulation Test Technology of Sichuan, Xihua University, Chengdu 610039, China
[4] School of Mechanics and Engineering Science, Shanghai University, Shanghai 200444, China

Abstract. An active inerter-based suspension with acceleration feedback control is proposed in this paper, the time delay generated in the controllers and actuators is considered, which constitutes the time-delayed active inerter-based (TDA-IB) suspension. The dynamic equation of the TDA-IB suspension is established and is a neutral type of delay differential equation (NDDE) in which the time delay exists in the highest-order derivative. The stability analysis is conducted by calculating the number of unstable characteristic roots based on the definite integral stability method, the stable and unstable regions are determined. The effect of time delay and feedback gain on the dynamic performance of the TDA-IB suspension under harmonic, random, and shock excitations is studied in detail and compared with the parallel-connected inerter-based (PC-IB) and traditional suspensions. The results show that the TDA-IB suspension is asymptotically stable for smaller feedback gain and time delay, through increasing the feedback gain, the stable regions shrink, and a smaller time delay could cause the system to become unstable. Furthermore, the time delay could regulate the resonance peak around the unsprung mass natural frequency and generate multiple high-frequency resonance peaks. If the time delay is chosen appropriately and falls into the stable range, the TDA-IB suspension could improve the dynamic performance for the suspension stroke and dynamic tire load while having a deterioration for the vehicle body acceleration compared with the PC-IB and traditional suspensions.

Key words: active inerter-based suspension; acceleration feedback control; dynamic performance; stability analysis; time delay.

1. INTRODUCTION

The suspension has a major effect on vehicle dynamics, it directly affects the comfort of the vehicle ride, road holding, and handling stability. The further improvement of the vehicle dynamics is restricted by the inherent structure of the traditional suspension, which is composed of damper and spring [1–3]. The inerter-based suspension is a suspension recently put forward and widely considered, which comprises damper, spring, and inerter [4]. Inerter is a device with two freely moving terminals and its generated force is proportional to the relative acceleration. The proportional constant is denoted as inertance with a unit of a kilogram. Inerter possesses the mass amplification effect, and it would supply a quite larger inertance compared with its own mass, which could increase the inertial of the total dynamic system instead of increasing the mass. Therefore, it is an efficient vibration attenuation structure because of its mechanical property. The inerter-based suspension could enhance the dynamics of the traditional suspension via devising different arrangements of damper, spring, and inerter, but at the expense of sophisticated configuration arrangements.

The inerter-based suspension could be divided into three categories: passive, semi-active, and active. The passive inerter-based suspension is composed of a passive damper, spring, and inerter. Wang *et al.* [5], Zhang *et al.* [6], and Liu *et al.* [7] studied the dynamic performance of the passive inerter-based suspension and found it could further improve the ride comfort and minimize road damage compared with the traditional suspension. The passive inerter-based suspension has high reliability and cost-effective characteristics and requires no input energy, while the dynamic performance is restricted compared with the semi-active and active ones.

The semi-active inerter-based (SA-IB) suspension comprises controllable elements, for instance, semi-active damper [8] or semi-active inerter [9]. The ball-screw, rack-and-pinion and fluid inerters are three mainly used inerters. If the inertance is fixed, the inerter is passive; otherwise, if inertance could be adjusted, the inerter is semi-active. Lazarek *et al.* [10, 11] proposed an inerter equipped with a continuously variable transmission (CVT), which could enable the step-free changes of inertance by varying the transmission ratio of the CVT. Faraj *et al.* [12] designed a ball-screw inerter with a variable thread

*e-mail: wangy1921@126.com

Manuscript submitted 2021-05-24, revised 2021-12-09, initially accepted for publication 2022-01-20, published in April 2022.

led to change the inertance for mitigating the impact loads. The semi-active inerter could be also achieved by designing a ball-screw or rack-and-pinion inerter with a controllable inertia flywheel [13] or devising tubes with different diameters and using electromagnetic valves to control them in the fluid inerter [14]. Chen *et al.* [13] applied both semi-active damper and semi-active inerter in the SA-IB suspension and proposed the feedback control method, which could enhance vehicle ride comfort and road holding. Zhang *et al.* [14] designed a continuously adjusted semi-active inerter and proposed a modified skyhook-inertance control method, showing that the SA-IB suspension could reduce the peak value in the low-frequency band. Zhang *et al.* [15] constructed an SA-IB suspension with a semi-active damper according to the skyhook, ground hook, and hybrid control methods, studied its dynamic behaviors, and found its dynamic performance is better compared with the passive inerter-based suspension. Hu *et al.* [16] proposed the continuous and on-off control methods for the semi-active inerter in SA-IB suspension to simulate the ideal skyhook inerter, indicated that it could improve the vehicle ride comfort. Wang *et al*. [17] proposed the acceleration-velocity-based switch control method according to the mechanical property of semi-active inerter, utilized it in SA-IB suspension to enhance the dynamic performance.

The active inerter-based suspension employs a controllable actuator to generate the desired force [18, 19], it provides better dynamic performance compared with the passive and semi-active ones, although requires the most energy. He *et al.* [20] proposed an active inerter-based suspension using the skyhook control and found it could achieve a better vehicle ride comfort. The active control strategies including sliding mode control, $H\infty$ control, optimal control and adaptive control strategies that used in the traditional active suspension system could be also utilized in the active inerter-based suspension to improve the dynamic performance. Here the acceleration feedback control is considered, which is based on the mechanical property of the inerter, this control strategy is simple and could be easily achieved in practical engineering [21,22]. Through constructing different arrangements of damper, spring, and inerter or adding another element, the inerter-based suspension may have various types. Here the active inerter-based suspension is based on the parallel-connected (PC) configuration. The damper, spring, and inerter is in PC, this configuration is simple and space efficient.

In the active inerter-based suspension, there exists unavoidable time delay in the controllers and actuators, which generates in the procedure of measuring the vehicle motion parameters, determining, and calculating the control methods, and achieving the control force. The time delay may cause the dynamic response to be more complicated, degenerate the dynamic performance, or make the dynamic system unstable; otherwise, if the time delay is chosen appropriately, the dynamic performance could be improved significantly. For the acceleration feedback control, if the time delay exists, the dynamic equation of the active inerter-based suspension is a neutral type of delay differential equation (NDDE), which includes a time delay in the highest-order derivative [23]. Compared with the retarded type of delay differential equation (RDDE), in which the highest-order derivative has no time delay, the NDDE shows some particular features in the aspects of dynamic characteristic and stability [24]. Thus the time-delayed active inerter-based (TDA-IB) suspension is considered here, the effect of time delay and feedback gain on its dynamic performance is studied and the stability analysis is conducted, the main goal is to study whether the time delay could further enhance or deteriorate the dynamic performance. The contributions of this paper are: (a) An active inerter-based suspension with time-delayed acceleration feedback control is proposed, which considers the effect of time delay. (b) The stability of the TDA-IB suspension is conducted and the stable and unstable regions are determined. (c) The influence law of the time delay and feedback gain on the dynamical performance of the TDA-IB suspension is analyzed. (d) The dynamic performance of the TDA-IB suspension is compared with the PC-IB and traditional suspensions to show its advantages.

The remaining part of the paper is the following. In Section 2, an active inerter-based suspension with time-delayed acceleration feedback control is presented, its dynamic equation is established and the performance criteria for harmonic excitation is acquired. In Section 3, the stability analysis is studied, the corresponding stable and unstable regions are obtained. In Section 4, the dynamic response of the TDA-IB suspension subjected to harmonic, random, and shock excitations is studied, the effect of time delay and feedback gain on its dynamic performance is analyzed. Section 5 exhibits the conclusions.

2. THE TDA-IB SUSPENSION AND ITS MODELING

A quarter-vehicle model equipped with TDA-IB suspension is shown in Fig. 1, which is based on the PC configuration. m_s and m_u are the sprung and unsprung masses respectively, c is the damping of the suspension, k_t and k are the stiffness of the tire and suspension respectively, the inertance of the inerter is b, z_s and z_u are the displacements of the sprung and unsprung masses from the static equilibrium positions respectively, the road excitation displacement is z_r. For the acceleration feedback control, the active force u is proportional to the relative acceleration between the sprung and unsprung masses, it equals to $g \cdot (z_s'' - z_u'')$, where g denotes the feedback gain.

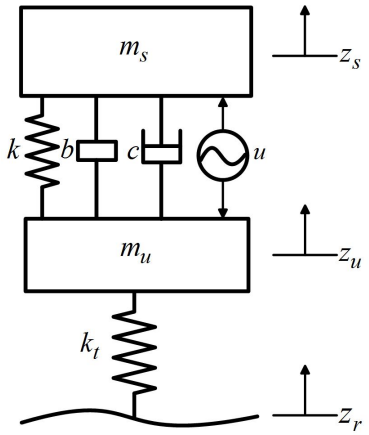

Fig. 1. Quarter-vehicle model equipped with TDA-IB suspension

The time delay generated in the controllers and actuators is considered and denoted as τ, the dynamic equation of the TDA-IB suspension is

$$\begin{cases} m_s z_s'' = -k(z_s - z_u) - c(z_s' - z_u') \\ \qquad - b(z_s'' - z_u'') - g[z_s''(t-\tau) - z_u''(t-\tau)], \\ m_u z_u'' = k(z_s - z_u) + c(z_s' - z_u') + b(z_s'' - z_u'') \\ \qquad + g[z_s''(t-\tau) - z_u''(t-\tau)] - k_t(z_u - z_r). \end{cases} \tag{1}$$

Rewriting equation (1) in a matrix form

$$\boldsymbol{M}_m \boldsymbol{Z}'' + \boldsymbol{M}_g \boldsymbol{Z}''(t-\tau) + \boldsymbol{C}\boldsymbol{Z}' + \boldsymbol{K}\boldsymbol{Z} = \boldsymbol{G}, \tag{2}$$

where

$$\begin{gathered} \boldsymbol{M}_m = \begin{bmatrix} m_s + b & -b \\ -b & m_u + b \end{bmatrix}, \quad \boldsymbol{M}_g = \begin{bmatrix} g & -g \\ -g & g \end{bmatrix}, \\ \boldsymbol{C} = \begin{bmatrix} c & -c \\ -c & c \end{bmatrix}, \quad \boldsymbol{K} = \begin{bmatrix} k & -k \\ -k & k + k_t \end{bmatrix}, \quad \boldsymbol{Z} = \begin{bmatrix} z_s \\ z_u \end{bmatrix}, \\ \boldsymbol{Z}(t-\tau) = \begin{bmatrix} z_s(t-\tau) \\ z_u(t-\tau) \end{bmatrix}, \quad \boldsymbol{G} = \begin{bmatrix} 0 \\ k_t z_r \end{bmatrix}. \end{gathered} \tag{3}$$

Considering the road excitation as the harmonic excitation, where $z_r = z_{rm}\cos(\omega t)$ with ω denoted as the excitation frequency and z_{rm} represented as the displacement amplitude. Using the Laplace transformed method yields the dynamic response of the TDA-IB suspension

$$\begin{aligned} z_s &= \frac{k_t z_r[(b+ge^{-\tau s})s^2 + cs + k]}{\begin{array}{l}[(m_s+m_u)(b+ge^{-\tau s}) + m_s m_u]s^4 + (m_s+m_u)cs^3 \\ +[m_s k_t + (m_s+m_u)k + (b+ge^{-\tau s})k_t]s^2 + ck_t s + kk_t\end{array}}, \\ z_u &= \frac{k_t z_r[(m_s+b+ge^{-\tau s})s^2 + cs + k]}{\begin{array}{l}[(m_s+m_u)(b+ge^{-\tau s}) + m_s m_u]s^4 + (m_s+m_u)cs^3 \\ +[m_s k_t + (m_s+m_u)k + (b+ge^{-\tau s})k_t]s^2 + ck_t s + kk_t\end{array}}, \end{aligned} \tag{4}$$

where s is the Laplace variable. In this paper, the dynamic performance of the TDA-IB suspension is evaluated by three performance criteria: vehicle body acceleration, defined as the acceleration of the sprung mass, it is concerned with the vehicle ride comfort; suspension stroke, defined as the relative displacement of the sprung and unsprung masses, it should be maintained within particular limits to avoid the components striking the limit blocks; dynamic tire load, defined as the force which equals the stiffness of the tire multiplying the relative displacement of the unsprung mass and road excitation, it corresponds to the road holding [25]. Based on the definition, the three performance criteria are

$$J_{VBA} = s^2 z_s = \frac{k_t z_r s^2[(b+ge^{-\tau s})s^2 + cs + k]}{\left\{\begin{array}{l}[(m_s+m_u)(b+ge^{-\tau s}) + m_s m_u]s^4 \\ +(m_s+m_u)cs^3 \\ +[m_s k_t + (m_s+m_u)k \\ +(b+ge^{-\tau s})k_t]s^2 + ck_t s + kk_t\end{array}\right\}}, \tag{5a}$$

$$\begin{aligned} J_{SSS} &= |z_s - z_u| \\ &= \frac{k_t z_r m_s s^2}{\left\{\begin{array}{l}[(m_s+m_u)(b+ge^{-\tau s}) + m_s m_u]s^4 \\ +(m_s+m_u)cs^3 \\ +[m_s k_t + (m_s+m_u)k \\ +(b+ge^{-\tau s})k_t]s^2 \\ +ck_t s + kk_t\end{array}\right\}}, \end{aligned} \tag{5b}$$

$$\begin{aligned} J_{DTL} &= k_t|z_u - z_r| \\ &= k_t z_r \frac{\left\{\begin{array}{l}[(m_s+m_u)(b+ge^{-\tau s}) + m_s m_u]s^4 \\ +(m_s+m_u)cs^3 + (m_s+m_u)ks^2\end{array}\right\}}{\left\{\begin{array}{l}[(m_s+m_u)(b+ge^{-\tau s}) + m_s m_u]s^4 \\ +(m_s+m_u)cs^3 \\ +[m_s k_t + (m_s+m_u)k + (b+ge^{-\tau s})k_t]s^2 \\ +ck_t s + kk_t\end{array}\right\}} \end{aligned} \tag{5c}$$

denoting $s = j\omega$, where j is the complex variable, substituting it into equations (4) and (5) yields

$$z_s(\omega) = \frac{k_t z_{rm}\sqrt{\begin{array}{l}[k - (b + g\cos\omega\tau)\omega^2]^2 \\ +[c\omega + (g\sin\omega\tau)\omega^2]^2\end{array}}}{\sqrt{\begin{array}{l}\{kk_t - [m_s k_t + (m_s+m_u)k \\ +(b+g\cos\omega\tau)k_t]\omega^2 \\ +[(m_s+m_u)(b+g\cos\omega\tau) + m_s m_u]\omega^4\}^2 \\ +\{ck_t\omega + k_t g\omega^2\sin\omega\tau \\ -(m_s+m_u)c\omega^3 - (m_s+m_u)g\omega^4\sin\omega\tau\}^2\end{array}}}, \tag{6a}$$

$$z_u(\omega) = \frac{k_t z_{rm}\sqrt{\begin{array}{l}[k - (g\cos\omega\tau + b + m_s)\omega^2]^2 \\ +[c\omega + (g\sin\omega\tau)\omega^2]^2\end{array}}}{\sqrt{\begin{array}{l}\{kk_t - [m_s k_t + (m_s+m_u)k \\ +(b+g\cos\omega\tau)k_t]\omega^2 \\ +[(m_s+m_u)(b+g\cos\omega\tau) + m_s m_u]\omega^4\}^2 \\ +\{ck_t\omega + k_t g\omega^2\sin\omega\tau \\ -(m_s+m_u)c\omega^3 - (m_s+m_u)g\omega^4\sin\omega\tau\}^2\end{array}}}, \tag{6b}$$

$$J_{VBA}(\omega) = \frac{\omega^2 k_t z_{rm}\sqrt{\begin{array}{l}[k - (b + g\cos\omega\tau)\omega^2]^2 \\ +[c\omega + (g\sin\omega\tau)\omega^2]^2\end{array}}}{\sqrt{\begin{array}{l}\{kk_t - [m_s k_t + (m_s+m_u)k \\ +(b+g\cos\omega\tau)k_t]\omega^2 \\ +[(m_s+m_u)(b+g\cos\omega\tau) + m_s m_u]\omega^4\}^2 \\ +\{ck_t\omega + k_t g\omega^2\sin\omega\tau \\ -(m_s+m_u)c\omega^3 - (m_s+m_u)g\omega^4\sin\omega\tau\}^2\end{array}}}, \tag{6c}$$

$$J_{SSS}(\omega)=\frac{k_t z_{rm} m_s \omega^2}{\sqrt{\begin{aligned}&\{kk_t-[m_s k_t+(m_s+m_u)k\\&+(b+g\cos\omega\tau)k_t]\omega^2\\&+[(m_s+m_u)(b+g\cos\omega\tau)+m_s m_u]\omega^4\}^2\\&+\{ck_t\omega+k_t g\omega^2\sin\omega\tau\\&-(m_s+m_u)c\omega^3-(m_s+m_u)g\omega^4\sin\omega\tau\}^2\end{aligned}}}, \quad (6d)$$

$$J_{DTL}(\omega)=\frac{k_t z_{rm}\sqrt{\begin{aligned}&\{-(m_s+m_u)k\omega^2\\&+[(m_s+m_u)(b+g\cos\omega\tau)+m_s m_u]\omega^4\}^2\\&+\{(m_s+m_u)c\omega^3\\&+(m_s+m_u)g\omega^4\sin\omega\tau\}^2\end{aligned}}}{\sqrt{\begin{aligned}&\{kk_t-[m_s k_t+(m_s+m_u)k\\&+(b+g\cos\omega\tau)k_t]\omega^2\\&+[(m_s+m_u)(b+g\cos\omega\tau)+m_s m_u]\omega^4\}^2\\&+\{ck_t\omega+k_t g\omega^2\sin\omega\tau\\&-(m_s+m_u)c\omega^3-(m_s+m_u)g\omega^4\sin\omega\tau\}^2\end{aligned}}}. \quad (6e)$$

Denote δ as the inertance-to-mass ratio equal to b/m_s, σ as the non-dimensional feedback gain equal to g/m_s, the structural parameter values of the TDA-IB suspension are shown in Table 1, which is based on a mature traditional suspension for a commercial vehicle.

Table 1
Structural parameter values of the TDA-IB suspension

m_u	m_s	k_t	k	c
40 [kg]	320 [kg]	190 [kN/m]	22 [kN/m]	1000 [Ns/m]

The dynamic response of the TDA-IB suspension obtained using the Laplace transformed method is compared with the numerical method and is shown in Fig. 2. The function ddensd in Matlab is adopted to solve equation (1) to obtain the numerical results, it is observed that the analytical results are in good agreement with numerical results, which shows that using the Laplace transformed method to obtain the analytical results could denote the true dynamic responses.

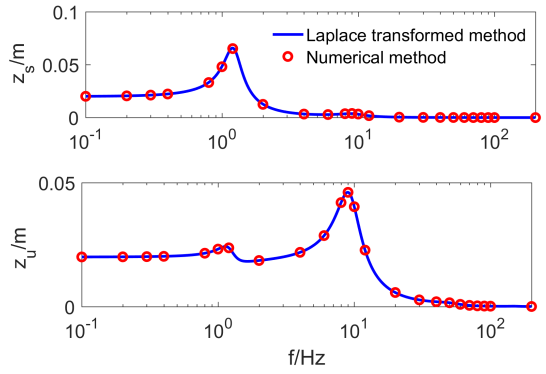

Fig. 2. Comparison between Laplace transformed method and numerical method of the dynamic response for the TDA-IB suspension ($\delta=0.01$, $\sigma=0.05$, $\tau=0.01$ [s], $z_r=0.02\cos(2\pi ft)$)

3. STABILITY ANALYSIS

The dynamic equation of the TDA-IB suspension is an NDDE in which the time delay exists in the highest-order derivative (see equation (2)), it could display particular characteristics compared with the RDDE in the perspective of stability. The NDDE could have infinite characteristic roots in the right-half complex plane while the RDDE has the finite ones. If all the real parts of the characteristic roots are negative, the RDDE is asymptotically stable, while the NDDE would not be stable as this condition is satisfied, because there could exist accumulation points in the imaginary axis. These accumulation points are usually discontinuous with the time delay and a perturbation of time delay could cause the NDDE to lose stability. Several methods have been proposed to analyze the stability of the NDDE, for instance, the Lyapunov–Krasovskii functional method [26], D-subdivision method [27], semi-discretization method [28], cluster treatment of characteristic roots method [29], stability switch method [30] and definite integral stability method [31]. Here the definite integral stability method is adopted, it originates from the argument principle and computes the number of unstable characteristic roots via an integral within a limited interval. The lower limit of the integral is zero and the upper limit could be conveniently defined, therefore it is effective in determining the stability of the NDDE and obtaining the corresponding stable and unstable regions.

Then the principle of definite integral stability method is introduced, considering a general form of the linear NDDE as

$$x'(t)+\sum_{k=1}^{m}Q_k x'(t-\tau_k)=Px(t)+\sum_{k=1}^{m}R_k x(t-\tau_k), \quad (7)$$

where $x\in R^n$ and P, Q_k, $R_k\in R^{n\times n}$ and $\tau_i\geq 0$ denotes the time delay, the characteristic equation of equation (7) is

$$f(\lambda)=\lambda^n+\sum_{k=1}^{n}\alpha_k\left(e^{-\lambda\tau_1},\ \ldots,\ e^{-\lambda\tau_m}\right)\lambda^{n-k}, \quad (8)$$

where λ is the characteristic root and $\alpha_k(e^{-\lambda\tau_1},\ldots,e^{-\lambda\tau_m})$, $k=0,1,\ldots,n$ are real polynomials. Equation (7) is an NDDE if there exists at least one Q_i not equal to zero that denotes $\alpha_0(e^{-\lambda\tau_1},\ldots,e^{-\lambda\tau_m})\neq 0$, while is an RDDE if all Q_i equal zero that denotes $\alpha_0(e^{-\lambda\tau_1},\ldots,e^{-\lambda\tau_m})\equiv 0$. For the NDDE, the characteristic roots could have accumulation points in the imaginary axis, so the dynamic system is asymptotically stable if and only if all the characteristic roots have negative real parts and are bounded away from the imaginary axis. The latter condition maintains if

$$\sup_{\Re(\lambda)>0,\ |\lambda|\to\infty}\left|\alpha_0(e^{-\lambda\tau_1},\ldots,e^{-\lambda\tau_m})\right|<1, \quad (9)$$

where the function $\Re$ denotes the real part of λ, the formula is true if $\alpha_0(e^{-\lambda\tau_1},\ldots,e^{-\lambda\tau_m})\equiv 0$.

Suppose that there are no characteristic roots in the imaginary axis for equation (8), denote N as the corresponding number of unstable characteristic roots in the right-half complex

plane, which could be determined by using the argument principle. Denote $\Delta_c \arg(f(\lambda))$ as the argument change over the closed-loop curve C shown in Fig. 3, which is given as

$$N = \lim_{R\to\infty} \frac{\Delta_c \arg(f(\lambda))}{2\pi} = \lim_{R\to\infty} \frac{1}{2\pi j} \oint_c \frac{f'(\lambda)}{f(\lambda)} \mathrm{d}\lambda, \tag{10}$$

where $C_1 : \lambda = Re^{j\theta}$, $\theta \in (-\pi/2, \pi/2)$, $C_2 : \lambda = j\omega$, $\omega \in (-R, R)$.

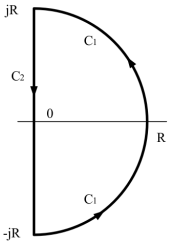

Fig. 3. The integral closed loop curve C

The NDDE is asymptotically stable if and only if the number of unstable characteristic roots equals zero ($N = 0$), while it is difficult to use equation (10) to calculate N directly. Assume that N is an integer, it has been proved that N could be determined by using the following formula

$$N = \text{round}\left(\frac{n}{2} - \frac{1}{\pi}\int_0^T \Re\left(\frac{f'(j\omega)}{f(j\omega)}\right) d\omega\right), \tag{11}$$

where round means the rounding function and T is a larger value.

Theorem 1. Suppose that there exist no characteristic roots in the imaginary axis for $f(\lambda)$ and condition (9) satisfies, the NDDE is asymptotically stable if and only if the number of unstable characteristic roots equals zero, it indicates $N = 0$ and is determined by equation (11).

Being aware that when using Theorem 1 and calculating N to judge the stability of NDDE, the upper limit of the integral function should be selected properly, we denote the following formula

$$j^{-n} f(j\omega) = H(\omega) + jI(\omega), \tag{12}$$

where $H(\omega)$ and $I(\omega)$ are the real and imaginary parts of the function $j^{-n}f(j\omega)$ respectively, and are composed of

$$\begin{aligned} H(\omega) &= (1 + h_0(\omega))\omega^n + \sum_{k=1}^{n} h_k(\omega)\omega^{n-k}, \\ I(\omega) &= (1 + i_0(\omega))\omega^n + \sum_{k=1}^{n} i_k(\omega)\omega^{n-k}, \end{aligned} \tag{13}$$

where $h_k(\omega)$, $i_k(\omega)$, $k = 0, 1, \ldots, n$ are functions about $\sin(\omega\tau_j)$, $\cos(\omega\tau_j)$, $j = 0, 1, \ldots, m$. According to condition (9), the leading coefficient of $H(\omega)$ is positive, which demonstrates that $H(\omega)$ is larger than zero for larger ω, therefore the number of positive roots for $H(\omega)$ should be finite. The functions $f(j\omega)$, $H(\omega)$, $I(\omega)$ have the following relationship

$$\Re\left(\frac{f'(j\omega)}{f(j\omega)}\right) = \frac{\mathrm{d}}{\mathrm{d}\omega} \arctan\frac{I(\omega)}{H(\omega)}. \tag{14}$$

Theorem 2. Suppose that there exist no characteristic roots in the imaginary axis for $f(\lambda)$ and condition (9) satisfies, denote $T_0(\tau_1, \ldots, \tau_m)$ as the maximum positive root of $H(\omega)$, then for all $T > T_0(\tau_1, \ldots, \tau_m)$, N satisfies equation (11) if $H(\omega)$ has no positive roots, select $T = 0$.

The critical upper limit defined in Theorem 2 depends on the structural parameters of the dynamic system and time delay, while it could be also parameter independent. Each coefficient $h_k(\omega)$ of the function $H(\omega)$ contains the trigonometric functions $\sin(\omega\tau_j)$ and $\cos(\omega\tau_j)$, so it has an infimum $\inf h_k(\omega)$ about the time delays $\tau_1, \ldots, \tau_m$, which are independent of all time delays. For any $\omega > 0$

$$\begin{aligned} H(\omega) \geq H_L(\omega) \overset{\text{def}}{=} &[1 + \inf h_0(\omega)]\omega^n \\ &+ \sum_{k=1}^{n} \inf h_k(\omega)\omega^{n-k}, \end{aligned} \tag{15}$$

where $H_L(\omega)$ is the lower limit of $H(\omega)$. Denote T_0 as the maximum positive root of $H_L(\omega)$, then it is independent of the time delays and not smaller than the maximum positive root of $H_L(\omega)$, therefore the following theorem maintains.

Theorem 3. Suppose that there exist no characteristic roots in the imaginary axis for $f(\lambda)$ and condition (9) satisfies, there exists a constant upper limit T_0 which is independent of the time delays, N satisfies equation (11) for all $T > T_0$.

In summary, the stability analysis of the NDDE using the definite integral stability method could be conducted in three steps, which are summarized in Fig. 4 and shown in the followings:

- **Step 1.** Based on the NDDE, calculate the characteristic equation $f(\lambda)$, determine the real parts $H(\omega)$ of the function $j^{-n}f(j\omega)$.
- **Step 2.** Determine the lower limit $H_L(\omega)$ of $H(\omega)$, calculate its maximum positive root T_0, compute the number of unstable characteristic roots N according to equation (11), where the upper limit T of the integral function in equation (11) is larger than T_0.
- **Step 3.** The neutral type of delay dynamic system is asymptotically stable if $N = 0$, while is unstable if $N > 0$.

The characteristic equation of the TDA-IB suspension is

$$\begin{aligned} f(\lambda) = &[(m_s + m_u)(b + ge^{-\lambda\tau}) + m_s m_u]\lambda^4 \\ &+ (m_s + m_u)c\lambda^3 \\ &+ [m_s k_t + (m_s + m_u)k + (b + ge^{-\lambda\tau})k_t]\lambda^2 \\ &+ ck_t\lambda + kk_t \end{aligned} \tag{16}$$

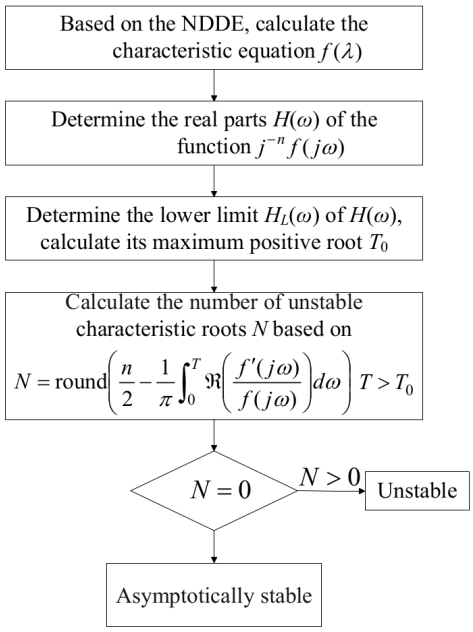

Fig. 4. The stability analysis process of the NDDE

the real parts of the function $j^{-n}f(j\omega)$ are

$$H(\omega) = kk_t - [m_s k_t + (m_s + m_u)k + (b + g\cos\omega\tau)k_t]\omega^2 + [(m_s + m_u)(b + g\cos\omega\tau) + m_s m_u]\omega^4 \quad (17)$$

the lower limit of $H(\omega)$ is

$$H_L(\omega) = kk_t - [m_s k_t + (m_s + m_u)k + (b + g)k_t]\omega^2 + [(m_s + m_u)(b - g) + m_s m_u]\omega^4 \quad (18)$$

then the maximum positive root T_0 and the number of unstable characteristic roots N could be obtained.

The stability of the TDA-IB suspension is determined by the structural parameters and time delay, which is based on its characteristic equation shown in (16), the number of unstable characteristic roots N can be obtained using equation (11). Equation (11) is an integral function of the frequency ω, the upper limit T of the integral function in equation (11) can be determined based on Theorem 3 and equation (18). It should be noted that the stability of the TDA-IB suspension is independent of the excitation frequency.

In Fig. 5, the inertance-to-mass ratio δ equals 0.01 and the other structural parameters of the TDA-IB suspension are cho-

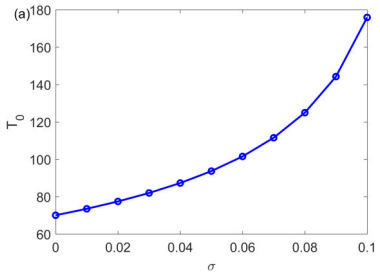

Fig. 5a

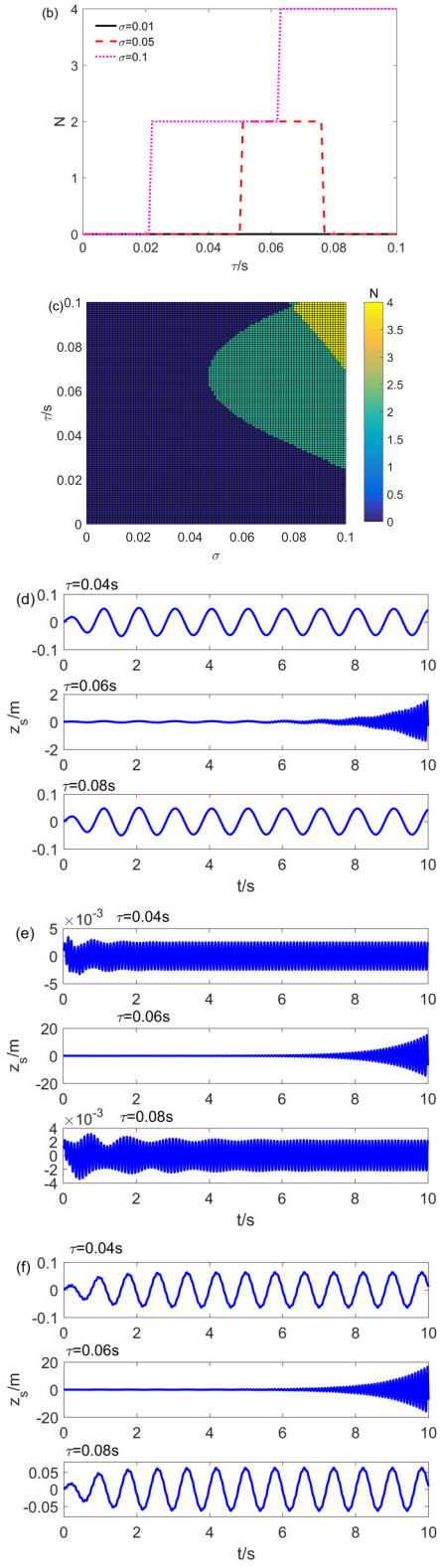

Fig. 5. (a) Maximum positive root T_0 with different σ, (b) number of unstable characteristic roots N with different σ and τ, (c) stable regions of the TDA-IB suspension, (d) displacement of the sprung mass with different τ for $\sigma = 0.05$ and $z_r = 0.02\cos(2\pi f_{ns}t)$, (e) displacement of the sprung mass with different τ for $\sigma = 0.05$ and $z_r = 0.02\cos(2\pi f_{nus}t)$ and (f) displacement of the sprung mass with different τ for $\sigma = 0.05$ and $z_r = 0.02\cos(2\pi f_{ns}t) + 0.02\cos(2\pi f_{nus}t)$ ($\delta = 0.01$)

sen the same values shown in Table 1. The maximum positive root T_0 of the function $H_L(\omega)$ with different feedback gain σ is displayed in Fig. 5a), which becomes larger as the feedback gain σ increases.

Choosing an upper limit T which is larger than T_0 and calculating the number of unstable characteristic roots N according to equation (11), the results are shown in Fig. 5b, the time delay τ is selected in the range $[0, 0.1]$. For smaller feedback gain σ ($\sigma = 0.01$), $N = 0$ which indicates that the TDA-IB suspension is asymptotically stable for the chosen structural parameters and the time delay range; by increasing the feedback gain $\sigma(\sigma = 0.05)$, two critical time delays exist ($\tau_1^* \approx 0.05$ [s], $\tau_2^* \approx 0.077$ [s]), the TDA-IB suspension is asymptotically stable if the time delay is chosen in the range $[0, 0.05] \cup [0.077, 1]$ with $N = 0$, while it is unstable if the time delay is chosen in the range (0.05, 0.077) with $N = 2$; for relatively larger feedback gain σ ($\sigma = 0.1$), one critical time delay exists ($\tau^* \approx 0.021$ [s]), the TDA-IB suspension is asymptotically stable if the time delay is smaller than τ^* with $N = 0$, while it is unstable if the time delay is larger than τ^* with $N > 0$ ($N = 2, 4$).

Figure 5c shows the stable and unstable regions of the TDA-IB suspension with $(\sigma, \tau) \in [0, 0.1] \times [0, 0.1]$, the colours exhibited in the figure denote the number of unstable characteristic roots N. As the time delay τ and feedback gain σ are chosen as smaller values, the TDA-IB suspension is asymptotically stable; if the feedback gain σ is smaller than 0.04, the time delay τ could be larger values (e.g. $\tau = 3$ [s]) to maintain the TDA-IB suspension stable, in this case, the presence of time delay could not alter the stability of the TDA-IB suspension. As the feedback gain σ increases, the stable regions shrink and even a smaller time delay could cause the TDA-IB suspension to become unstable, for example, if the feedback gain σ equals 0.1 and the time delay is chosen as 0.025 [s], the TDA-IB suspension would be unstable.

As the inertance-to-mass ratio δ equals 0.01, the two natural frequencies of the TDA-IB suspension equal 1.25 [Hz] and 11.59 [Hz] respectively ($f_{ns} = 1.25$ [Hz], $f_{nus} = 11.59$ [Hz]). The road excitation is harmonic excitation and chosen as $z_r = 0.02\cos(2\pi f_{ns} t)$, $z_r = 0.02\cos(2\pi f_{nus} t)$ and $z_r = 0.02\cos(2\pi f_{ns} t) + 0.02\cos(2\pi f_{nus} t)$ respectively, the displacement of the sprung mass with different time delays is shown in Figs. 5d, 5e and 5f respectively. The time delay τ is chosen as 0.04 [s], 0.06 [s] and 0.08 [s] respectively; the number of unstable characteristic roots N equals 0, 2, and 0 respectively, which falls into the stable, unstable, and stable regions respectively, which can be also seen in Figs. 5b and 5c. If the time delay τ equals 0.04 [s] or 0.08 [s], it falls into the stable range $[0, 0.05] \cup [0.077, 1]$; the displacement of the sprung mass is convergent and within a limited value as time increases for three road harmonic excitations. While if the time delay τ equals 0.06 [s], it is in the unstable range $(0.05, 0.077)$, the displacement of the sprung mass is divergent and becomes very large as time increases for three road harmonic excitations. Figures 5d, 5e, and 5f exhibit the stability of the TDA-IB suspension in the time domain, and the results are consistent with those shown in Fig. 5b and verify that the stability of the TDA-IB suspension is independent of the excitation frequency.

4. DYNAMIC RESPONSE ANALYSIS

4.1. Harmonic excitation

The harmonic excitation is considered first, which could exhibit the dynamic performance of TDA-IB suspension in the frequency domain. It has been shown in [17] that compared with the traditional suspension, the PC-IB suspension could enhance the dynamic performance in the low-frequency range while having a degeneration in the high-frequency range because the low-frequency resonance peak of the performance criteria becomes smaller while the high-frequency one increases significantly as the inertance-to-mass ratio δ increases. The TDA-IB suspension is based on the three-element PC configuration, therefore the corresponding inertance-to-mass ratio δ is set to be smaller values. In the following analysis, the inertance-to-mass ratio δ is chosen as 0.01.

Figure 6 shows the three performance criteria of the TDA-IB suspension with different time delays, the corresponding plots of the PC-IB and traditional ones are also displayed for

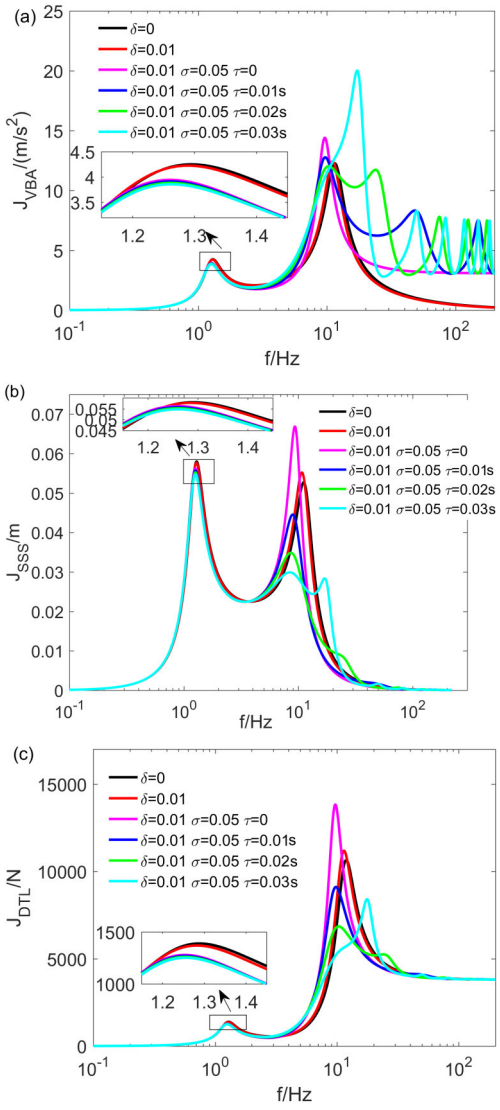

Fig. 6. Three performance criteria of the TDA-IB suspension with different τ under harmonic excitation: (a) vehicle body acceleration, (b) suspension stroke and (c) dynamic tire load ($z_{rm} = 0.02$ [m])

comparison. The time delay τ is chosen as 0.01 [s], 0.02 [s], and 0.03 [s] respectively, which falls into the stable range and maintains the TDA-IB suspension stability (see Fig. 5c). The frequency range is chosen as $[0.1, 200]$ in the logarithmic coordinate form, which aims to show the effect of time delay on the three performance criteria in the high-frequency range; it is also consistent with the dynamic response shown in Fig. 2.

The time delay has less effect on the resonance peak around the sprung mass natural frequency while affecting the resonance peak around the unsprung mass natural frequency greatly. As the time delay increases, the resonance peak around the sprung mass natural frequency is slightly reduced, while the resonance peak around the unsprung mass natural frequency first decreases and then increases significantly, especially for the vehicle body acceleration. It should be noted that there exist multiple high-frequency resonance peaks for the three performance criteria as the time delay exists, which is different from the two passive suspensions because the trigonometric functions $\sin(\omega\tau)$ and $cos(\omega\tau)$ exist in the formulas (see equation (6)). The effect of time delay is more obvious in the high-frequency range, especially for the vehicle body acceleration. The multiple high-frequency resonance peaks of the vehicle body acceleration are relatively larger values and are comparable to the one around the unsprung mass natural frequency, while for the other two performance criteria, they are relatively smaller. Therefore the time delay could regulate the resonance peak around the unsprung mass natural frequency and generate multiple high-frequency resonance peaks. The TDA-IB suspension could improve the suspension stroke and dynamic tire load while having a degeneration for the vehicle body acceleration compared with the two passive suspensions.

Figure 7 shows the three performance criteria of the TDA-IB suspension with different feedback gains. The feedback gain σ is chosen as 0.01, 0.05, and 0.08 respectively, the time delay τ is chosen as 0.01 [s], which also falls into the stable range and keeps the TDA-IB suspension stable. As the feedback gain σ increases, the resonance peak around the sprung mass natural frequency reduces slightly; the resonance peak around the unsprung mass natural frequency increases for the vehicle body acceleration while decreasing for the other two performance criteria, which is different from the counterparts of the PC-IB suspension. Due to the existence of time delay, multiple high-frequency resonance peaks exist for the three performance criteria and increase significantly as the feedback gain σ becomes larger.

While checking equation (6), it is found that by choosing appropriate structural parameters, time delay and feedback gain, the vehicle body acceleration and dynamic tire load of the TDA-IB suspension could equal zero for a certain excitation frequency when subjected to harmonic excitation, while the suspension stroke could equal zero if and only if the excitation frequency $\omega = 0$. If the vehicle body acceleration $J_{VBA} = 0$, it has

$$g = \frac{\sqrt{(k - b\omega^2)^2 + c^2\omega^2}}{\omega^2}, \qquad \tau = \frac{1}{\omega}\arctan\frac{c\omega}{b\omega^2 - k}. \tag{19}$$

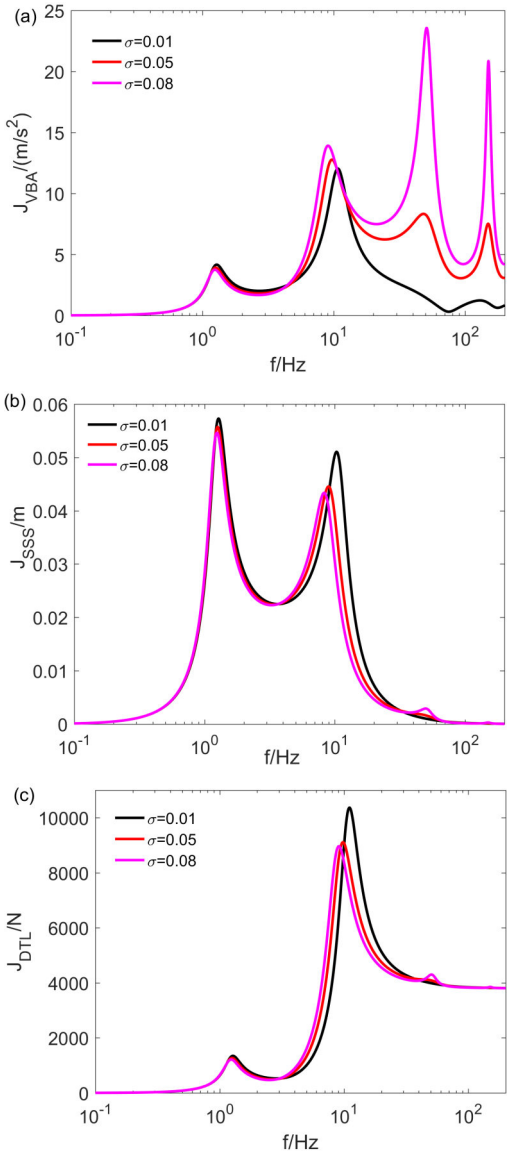

Fig. 7. Three performance criteria of the TDA-IB suspension with different σ under harmonic excitation: (a) vehicle body acceleration, (b) suspension stroke and (c) dynamic tire load ($\delta = 0.01$, $\tau = 0.01$ [s], $z_{rm} = 0.02$ [m])

Figure 8a shows the critical feedback gain σ and time delay τ, which decrease as the excitation frequency increases. The vehicle body acceleration could be set to zero in the sprung and unsprung mass natural frequencies respectively, the corresponding critical feedback gain σ and time delay τ are set to $\sigma_{cr1} = 1.1768$, $\tau_{cr1} = 0.7569$ [s] ($f_{ns} = 1.25$ [Hz]) and $\sigma_{cr2} = 0.0429$, $\tau_{cr2} = 0.0656$ [s] ($f_{nus} = 11.59$ [Hz]). The first set of feedback gain σ and time delay τ are relatively larger values, the TDA-IB suspension would be unstable, so the displacement of the sprung mass with the two sets of structural parameters and time delays are shown in Fig. 8b, the harmonic excitation is chosen as $z_r = 0.02\cos(2\pi f_{ns}t)$ and $z_r = 0.02\cos(2\pi f_{nus}t)$ respectively. The displacement of the sprung mass is divergent and very large as increasing the time, which indicates that the TDA-IB suspension is unstable for the chosen structural param-

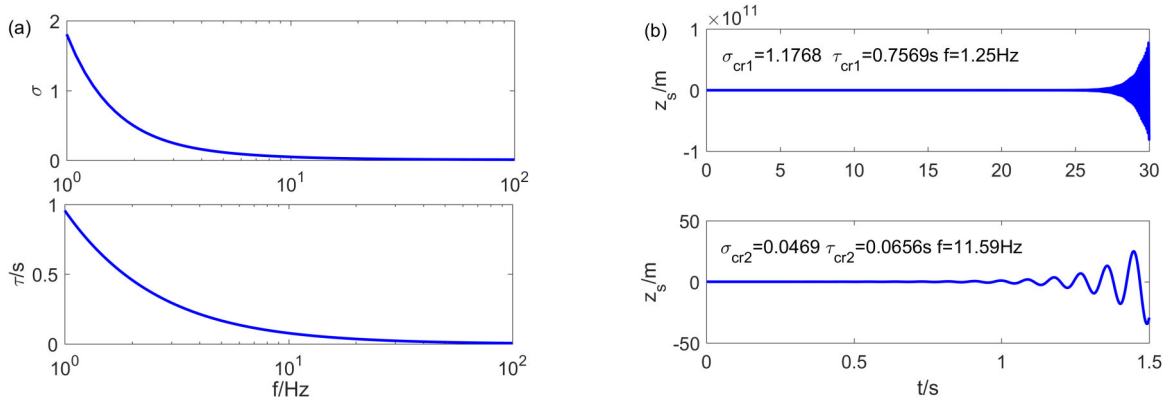

Fig. 8. (a) Critical feedback gain σ and time delay τ for $J_{VBA} = 0$, (b) displacement of the sprung mass as $J_{VBA} = 0$ in sprung and unsprung mass natural frequencies ($\delta = 0.01$)

eters and time delays, so the vehicle body acceleration cannot equal zero in the sprung and unsprung mass natural frequencies.

If the feedback gain σ is fixed, the excitation frequency ω and critical time delay τ where the vehicle body acceleration $J_{VBA} = 0$ could be obtained as

$$\omega = \begin{cases} \sqrt{\dfrac{k^2}{2kb - c}} & \text{if } g = b, \\ \sqrt{\dfrac{(2kb - c^2) \pm \sqrt{c^4 - 4kbc^2 + 4k^2g^2}}{2(b^2 - g^2)}} & \text{if } g \neq b, \end{cases}$$

$$\tau = \frac{1}{\omega} \arctan \frac{c\omega}{b\omega^2 - k}. \tag{20}$$

The inertance-to-mass ratio δ is chosen as 0.01 and the feedback gain σ is chosen as 0.015 and 0.02 respectively, the determined excitation frequency ω equals to 260.16 [rad/s] and 168.88 [rad/s] and the critical time delay τ equals to 0.0156 [s] and 0.0256 [s] respectively. The TDA-IB suspension is asymptotically stable for these structural parameters and time delays (see Fig. 5b), the resulting displacements are shown in Fig. 9a, the corresponding three performance criteria are displayed in Fig. 9b. The displacement of the sprung mass decreases to zero as time increases, the harmonic excitation could be totally reduced and cannot transfer to the sprung mass. The excitation frequency where the vehicle body acceleration $J_{VBA} = 0$ could be also clearly displayed in the respect of frequency domain (see Fig. 9b). For the TDA-IB suspension, if the above feedback gain σ and time delay τ are chosen as relatively smaller values, compared with the two passive suspensions, the resonance peak around the sprung and unsprung mass natural frequencies would be smaller.

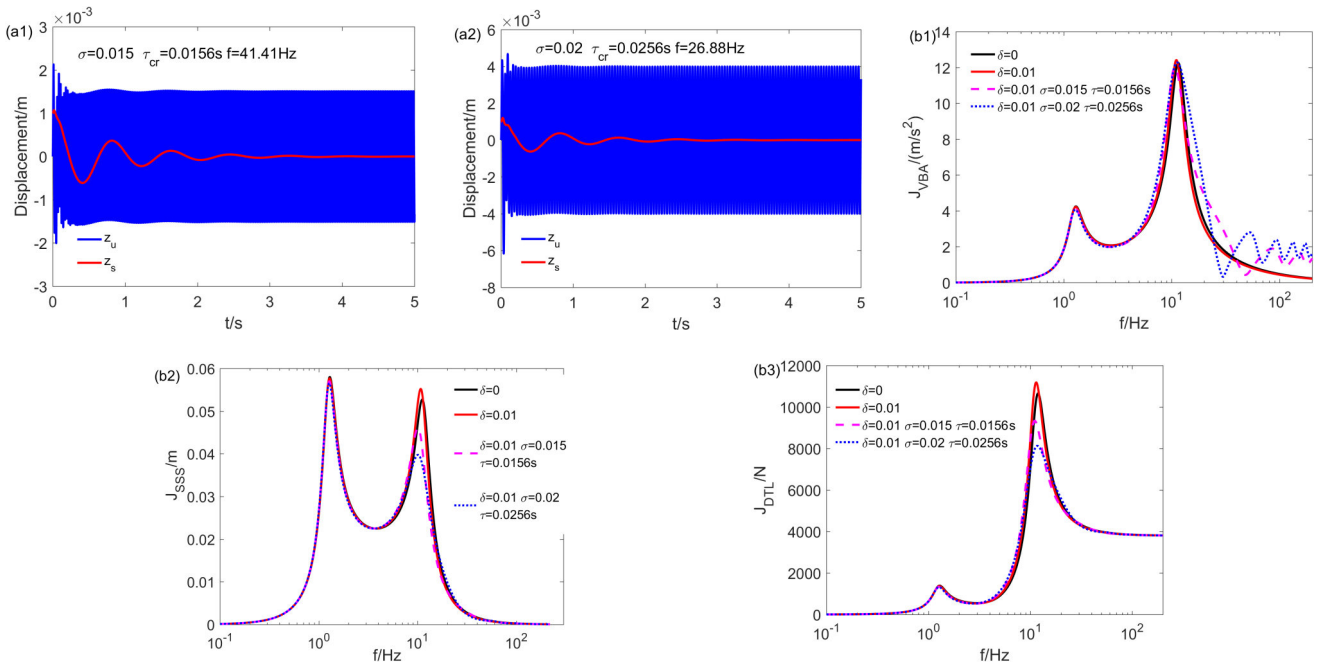

Fig. 9. (a) The displacements of the unsprung and sprung masses and (b) three performance criteria of the TDA-IB suspension with different σ and τ as $J_{VBA} = 0$ ($z_{rm} = 0.02$ [m])

If the dynamic tire load $J_{DTL}=0$, it has

$$g=\frac{\sqrt{[(m_s+m_u)(b\omega^2-k)+m_sm_u\omega^2]^2+[(m_s+m_u)c\omega]^2}}{(m_s+m_u)\omega^2},$$
$$\tau=\frac{1}{\omega}\arctan\left[\frac{(m_s+m_u)c\omega}{m_sm_u\omega^2+(m_s+m_u)(b\omega^2-k)}\right] \tag{21}$$

as the excitation frequency ω increases, the critical feedback gain σ first decreases then increases while the time delay τ decreases, this trend is displayed in Fig. 10a. In a certain parameter range, there exist two excitation frequencies for the same feedback gain σ where $J_{DTL}=0$, the corresponding lower and upper limits of the feedback gain σ are

$$\sigma_l=\frac{c\sqrt{(m_s+m_u)[4m_sm_uk+(m_s+m_u)(4kb-c^2)]}}{2(m_s+m_u)m_sk},$$
$$\sigma_u=\frac{(m_s+m_u)b+m_sm_u}{(m_s+m_u)m_s} \tag{22}$$

for chosen structural parameters, the two feedback gains equal 0.1103 and 0.1211 respectively, a small-time delay could cause the TDA-IB suspension to be unstable (see Fig. 6c). Setting the feedback gain σ to 0.115, which is within the range $(0.1103, 0.1211)$, the determined excitation frequency ω equals 28.83 [rad/s] and 62.79 [rad/s] and the critical time delay τ equals 0.152 [s] and 0.057 [s] respectively; setting the feedback gain σ to 0.125, the determined excitation frequency ω and critical time delay τ equal to 25.12 [rad/s] and 0.18 [s] respectively, the resulting displacement of the sprung mass is exhibited in Fig. 10b, which shows divergent tendency and is very large as the time increases. Therefore the TDA-IB suspension is unstable for the chosen structural parameters and time delays, the dynamic tire load cannot equal zero for this case.

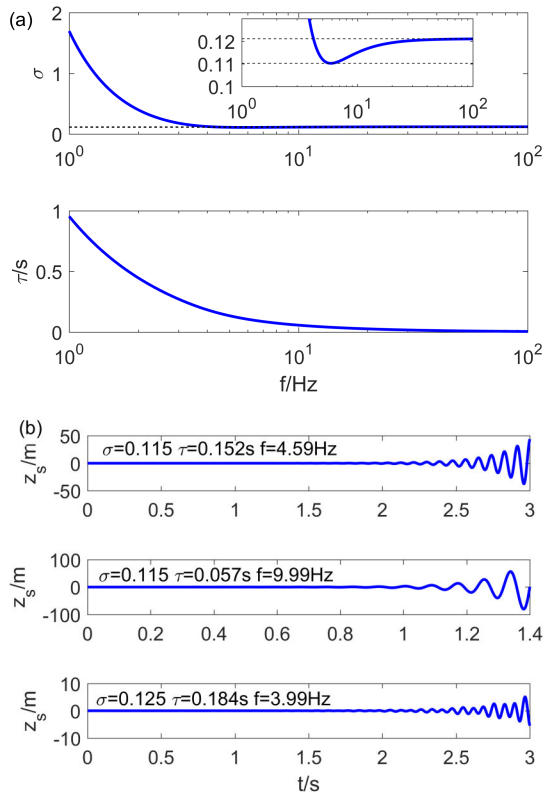

Fig. 10. (a) Critical feedback gain σ and time delay τ for $J_{DTL}=0$, (b) displacement of the sprung mass with different σ and τ as $J_{DTL}=0$ ($\delta=0.01$, $z_{rm}=0.02$ [m])

4.2. Random excitation

Then the random excitation is investigated, the road profiles could be characterized by the stationary zero-mean Gaussian random fields [32], the power spectral density (PSD) of the geometrical road profiles is given as

$$S_g(\Omega)=\begin{cases}S_g(\Omega_0)\left(\dfrac{\Omega}{\Omega_0}\right)^{-n_1}, & \text{if } \Omega\le\Omega_0,\\ S_g(\Omega_0)\left(\dfrac{\Omega}{\Omega_0}\right)^{-n_2}, & \text{if } \Omega\ge\Omega_0,\end{cases} \tag{23}$$

where Ω is spatial frequency, $\Omega=1/(2\pi)$ is reference spatial frequency, n_1 and n_2 are road roughness constants, the value of $S_g(\Omega_0)$ provides a measure for the roughness of the road. Assuming the vehicle traveling with a constant horizontal speed V over a given road, the road excitation displacement could be approximated by using the spectral representation method, which is given by

$$z_r(t)=\sum_{k=1}^{N_f}S_k\sin(k\omega_0t+\phi_k), \tag{24}$$

where k is the order of harmonic term as using the spectral representation method to denote the road random excitation, it is an integer and chosen in the ranges from 1 to N_f, the parameter N_f determines the considered frequency range for road random excitation. ω_0 is the fundamental temporal frequency and equals $(2\pi V)/l$, l is the length of the road segment. φ_k is treated as random variables and follows a uniform distribution in the interval 0.2π). $S_k=\sqrt{2S_g(k\Delta\Omega)\Delta\Omega}$, $\Delta\Omega=2\pi/l$ is the spatial frequency increment. For the class D road profiles (poor quality), $S_g(\Omega_0)=256\times10^{-6}$ [m^3]. The other parameters are chosen as $n_1=2$, $n_2=1.5$, $l=200$ [m], $N_f=200$ and $V=60$ [km/h].

Figure 11 shows the time history of three performance criteria for the TDA-IB suspension with different time delays under random excitation, the corresponding root mean square (RMS) values of the three performance criteria are displayed in Table 2, the structural parameters and time delays are the same with the harmonic excitation which maintains the system stable. For the PC-IB suspension, as the inertance-to-mass ratio δ is chosen as 0.01, the RMS value of the vehicle body acceleration is a bit smaller than that of the traditional one, which decreases by 3.37%; while the RMS values of the other two performance criteria are larger than the counterparts of the traditional one, which increase by 0.27% and 4.65% respectively; thus the adopted three-element PC configuration could further degenerate the dynamic performance of the traditional suspension, which is consistent with the results of the harmonic excitation shown in the frequency domain. For the TDA-IB suspension, as the time delay increases, the RMS value of the vehicle

body acceleration increases, while the RMS value of the other two performance criteria decreases, this tendency could be also predicted by those of the harmonic excitation. If the feedback gain $\sigma = 0.05$ and time delay $\tau = 0.02$ [s], the RMS value of the vehicle body acceleration increases by 16.53%, while the RMS values of the other two performance criteria decrease by 6.29% and 13.52% respectively compared with those of the traditional suspension. Therefore if the time delay is chosen appropriately and within the stable range, the TDA-IB suspension could improve the dynamic tire load significantly and suspension stroke slightly, while deteriorating the vehicle body acceleration compared with the two passive suspensions as subjected to random excitation.

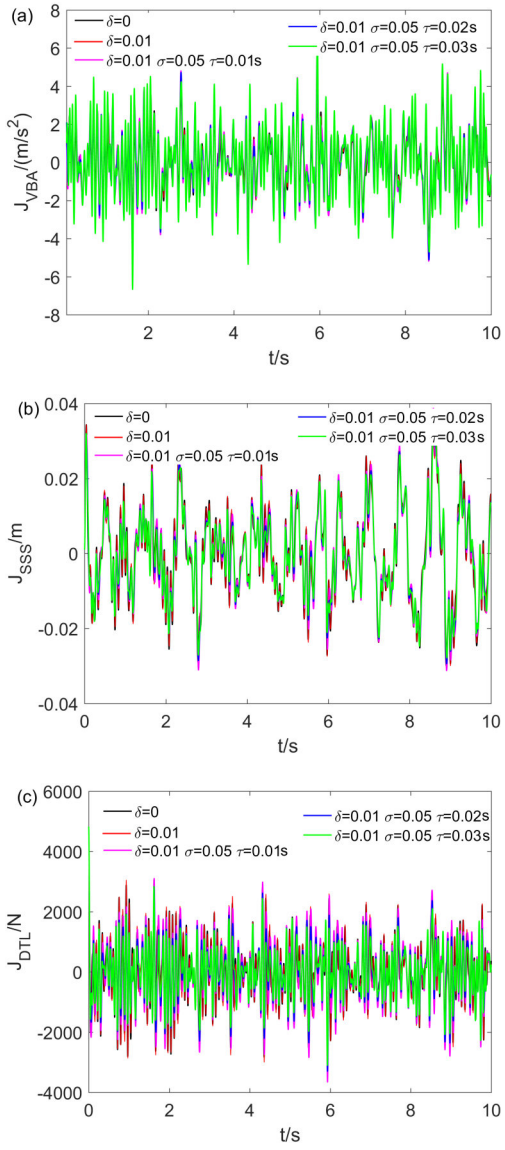

Fig. 11. Time history of three performance criteria for the TDA-IB suspension with different τ under random excitation: (a) vehicle body acceleration, (b) suspension stroke, and (c) dynamic tire load

Figure 12 shows the time history of three performance criteria for the TDA-IB suspension with different feedback gains under random excitation, the corresponding RMS values of the three performance criteria are exhibited in Table 3. As the feedback gain σ increases, the RMS value of the vehicle body acceleration increases, while the RMS value of the suspension stroke decreases slightly, the RMS value of the dynamic tire load first decreases and then increases.

Table 2
RMS values of three performance criteria for the TDA-IB suspension system with different τ under random excitation

	J_{VBA} [m/s^2]	Increase [%]	J_{SSS} [m]	Increase [%]	J_{DTL} [N]	Increase [%]
$\delta = 0$	1.4489	–	0.0119	–	1013.28	–
$\delta = 0.01$	1.4001	–3.37	0.0119	0.27	1060.41	4.65
$\delta = 0.01$ $\sigma = 0.05$ $\tau = 0.01$ [s]	1.6464	13.62	0.0115	–3.73	1024.54	1.11
$\delta = 0.01$ $\sigma = 0.05$ $\tau = 0.02$ [s]	1.6884	16.53	0.0112	–6.29	876.30	–13.52
$\delta = 0.01$ $\sigma = 0.05$ $\tau = 0.03$ [s]	1.8299	26.29	0.0111	–6.89	808.05	–20.25

Table 3
RMS values of three performance criteria for the TDA-IB suspension system with different σ under random excitation ($\delta = 0.01$, $\tau = 0.01$ [s])

	J_{VBA} [m/s^2]	J_{SSS} [m]	J_{DTL} [N]
$\sigma = 0.01$	1.4351	0.0118	1035.78
$\sigma = 0.05$	1.6464	0.0115	1024.54
$\sigma = 0.08$	1.8208	0.0113	1050.49

4.3. Shock excitation

As the vehicle drives on the road with a bump or discrete irregularity, it is subjected to shock excitation, three typical road excitation displacements applied for the suspension analysis with shock excitation are rounded step, rounded pulse, and oscillatory step [33], which are given as

$$\begin{aligned} z_r(t) &= z_{r\max}\left[1-(1+\gamma\omega_0 t)e^{-\gamma\omega_0 t}\right], \\ z_r(t) &= 0.25e^2 z_{r\max}(\gamma\omega_0 t)^2 e^{-\gamma\omega_0 t}, \\ z_r(t) &= 0.68684 z_{r\max}\left[1-(\cos(\gamma\omega_0 t) \right. \\ &\quad \left. +0.25\sin(\gamma\omega_0 t))e^{-\gamma\omega_0 t}\right] \end{aligned} \tag{25}$$

and shown in Fig. 13, where $z_{r\max}$ is the maximum road excitation displacement and is chosen as 0.02 [m], γ is the severity parameter and $\omega_0 = \sqrt{k/m_s}$. As the severity parameter γ is larger, it means a sharper irregularity or a hit with a higher velocity, here it represents the former.

The time history of three performance criteria for the PC-IB suspension with different inertance-to-mass ratios under shock

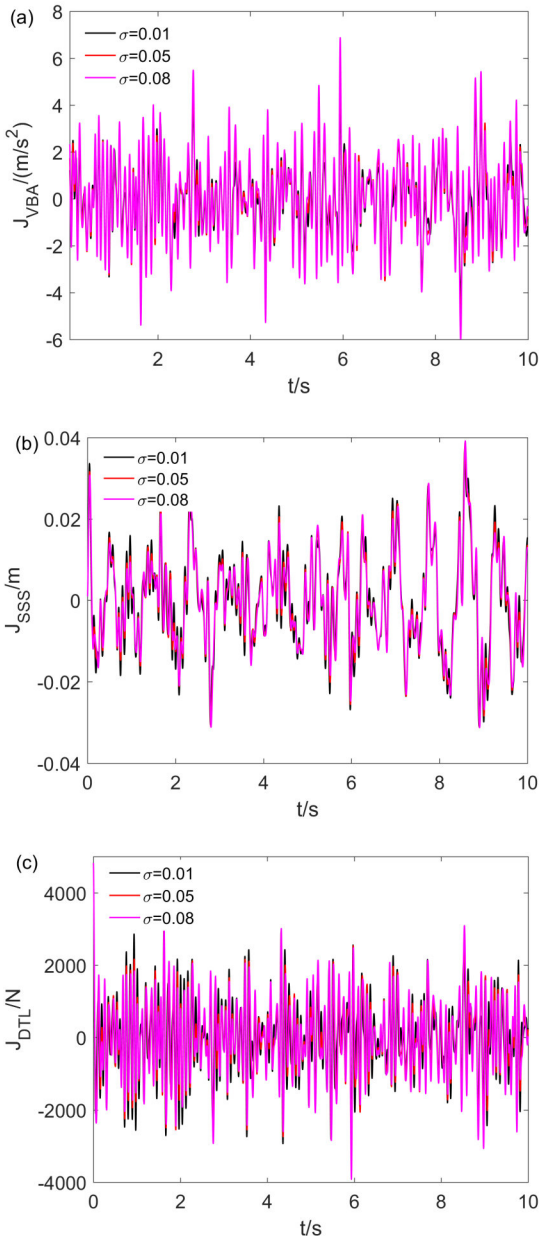

Fig. 12. Time history of three performance criteria for the TDA-IB suspension with different σ under random excitation: (a) vehicle body acceleration, (b) suspension stroke and (c) dynamic tire load ($\delta = 0.01$, $\tau = 0.01$ [s])

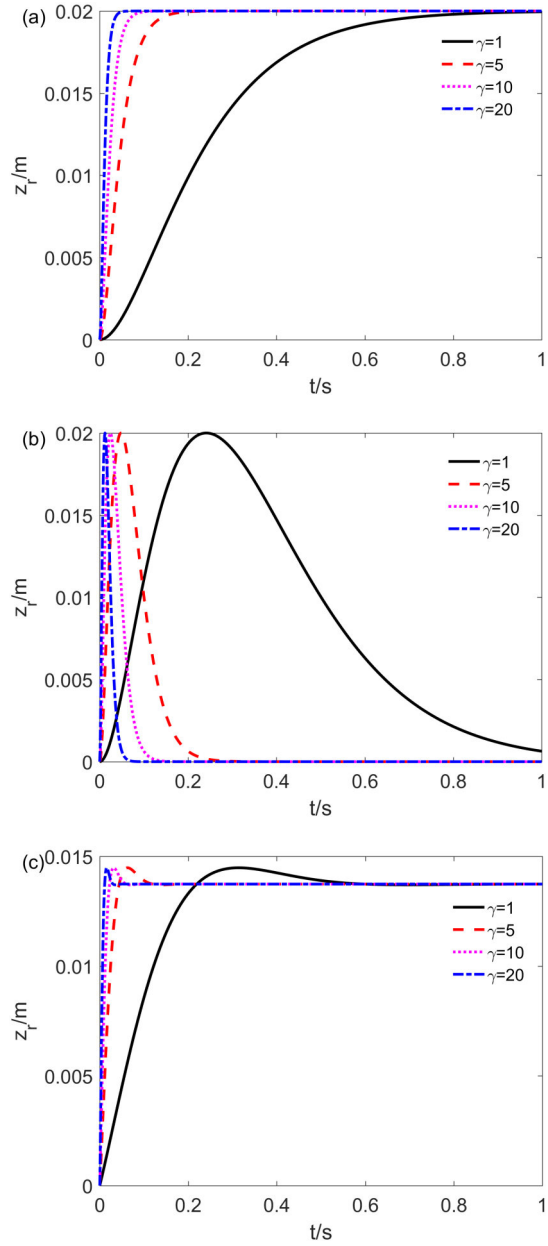

Fig. 13. Three typical types of road shock excitation: (a) rounded step, (b) rounded pulse, and (c) oscillatory step ($z_{r\max} = 0.02$ [m])

excitation is displayed in Fig. 14, where $\gamma = 5$ denotes less severe impact. The time history of three performance criteria fluctuates severer and takes more time to attenuate compared with the traditional suspension. In addition, there exist more peaks in the time history and the values become larger via increasing the inertance-to-mass ratio δ.

Figure 15 shows the maximum values of three performance criteria for PC-IB suspension with different γ and δ. If the PC-IB suspension is subjected to rounded step and oscillatory step excitations, the maximum values of three performance criteria first increase and then approach the fixed values with the increase in the severity parameter γ; if the rounded pulse excitation is imposed, the maximum values of three performance criteria first increase, reach the peak values and then decrease to the fixed values as increasing the severity parameter γ, which exhibits different tendency with the other shock excitations. By increasing the inertance-to-mass ratio δ, the maximum values of the vehicle body acceleration and dynamic tire load increase. For smaller severity parameter γ, the maximum value of the suspension stroke increases as the inertance-to-mass ratio δ increases, while showing the opposite tendency for larger severity parameter γ. As the severity parameter γ is small, the maximum values of three performance criteria are the same for the PC-IB and traditional suspensions; with the increase of the severity parameter γ, the maximum values of the vehicle body acceleration and dynamic tire load for the PC-IB suspension are larger than

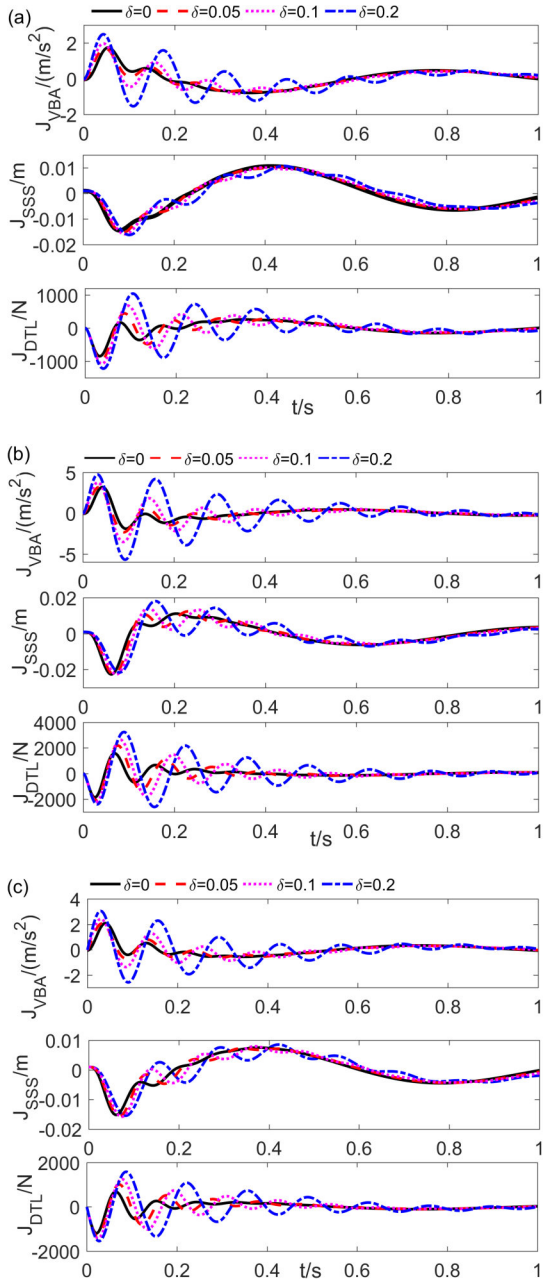

Fig. 14. Time history of three performance criteria for the PC-IB suspension with different δ under shock excitation: (a) rounded step, (b) rounded pulse, and (c) oscillatory step ($\gamma = 5$, $z_{r\max} = 0.02$ [m])

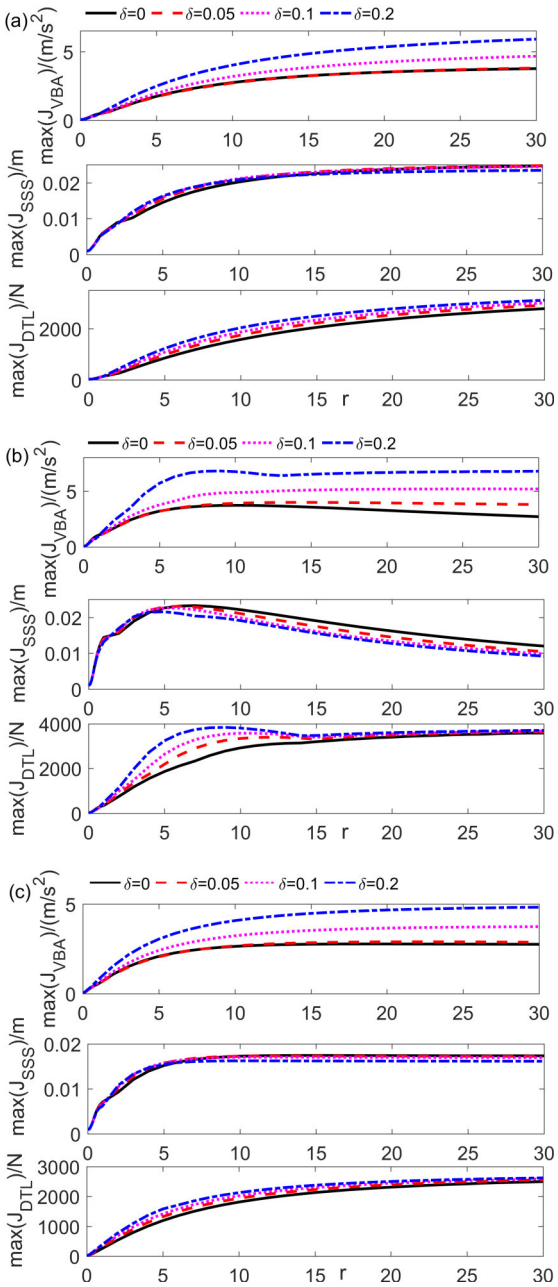

Fig. 15. The maximum values of three performance criteria for the PC-IB suspension with different γ and δ: (a) rounded step, (b) rounded pulse, and (c) oscillatory step ($z_{r\max} = 0.02$ [m])

those of the traditional one, while being smaller for the suspension stroke. Therefore, if the three typical types of road shock excitation are imposed, the PC-IB suspension degenerates the vehicle body acceleration and dynamic tire load more than the traditional suspension, while possibly enhancing the suspension stroke slightly for larger severity parameter γ.

The time history of three performance criteria for the TDA-IB suspension with different time delays under shock excitation is displayed in Fig. 16, the structural parameters and time delays are selected within the stable ranges, the severity parameter γ is also chosen as 5. As the time delay τ increases, the peak value of the vehicle body acceleration increases in the time history; while the peak values of the other performance criteria decrease, which indicates that the fluctuation is smoother and takes less time to attenuate than the PC-IB suspension.

Figure 17 shows the maximum values of three performance criteria for TDA-IB suspension with different γ and τ, the changing tendency for different γ is similar to the counterparts of the PC-IB suspension, so it is not elaborated on here, as we are more concerned with the effect of time delay. For smaller severity parameter γ (e.g. $\gamma < 1$), the time delay has little effect, the maximum values of the three performance criteria are almost the same with different time delays. For larger severity parameter γ, the maximum value of the vehicle body ac-

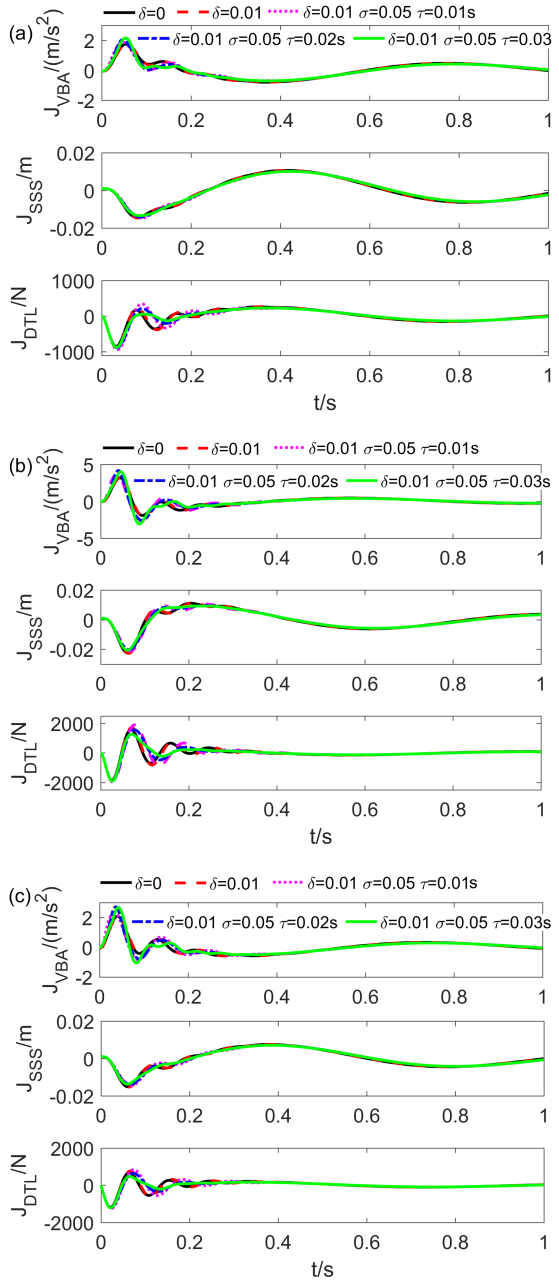

Fig. 16. Time history of three performance criteria for the TDA-IB suspension with different τ under shock excitation: (a) rounded step, (b) rounded pulse, and (c) oscillatory step ($\gamma = 5$, $z_{r\max} = 0.02$ [m])

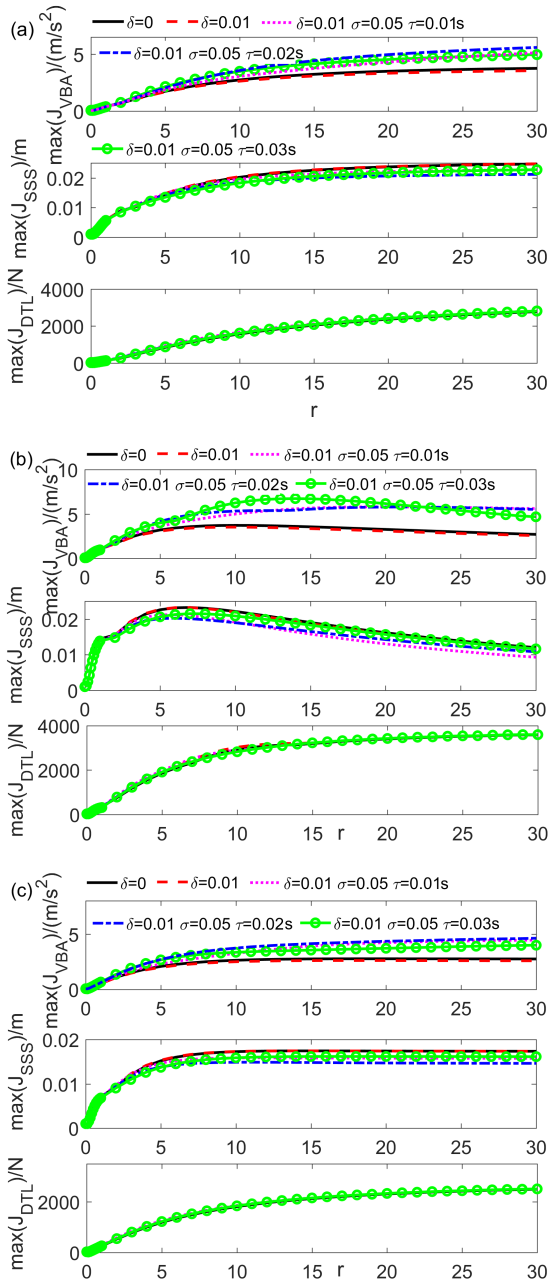

Fig. 17. The maximum values of three performance criteria for the TDA-IB suspension with different γ and τ: (a) rounded step, (b) rounded pulse, and (c) oscillatory step ($z_{r\max} = 0.02$ [m])

celeration first increases then decreases as increasing the time delay τ, which is also larger than that of the PC-IB and traditional suspensions; while the maximum values of the other performance criteria display the reverse tendency, which means they first decrease then increase as the time delay τ grows, the maximum value of the suspension stroke is smaller than the other two suspensions, the maximum value of the dynamic tire load is smaller than the counterpart of the PC-IB suspension and approach the value of the traditional one. Thus the TDA-IB suspension could further enhance the suspension stroke and dynamic tire load than the PC-IB suspension, while on the other hand, it degenerates the vehicle body acceleration.

The time history of three performance criteria for the TDA-IB suspension with different feedback gains under shock excitation is displayed in Fig. 18. As the severity parameter γ equals 5 and the feedback gain σ increases, the peak values of the three performance criteria become larger in the time history. Figure 19 shows the maximum values of three performance criteria for the TDA-IB suspension with different γ and σ. For the three shock excitations, as the feedback gain σ increases, the maximum value of the vehicle body acceleration increases, while the maximum value of the suspension stroke decreases, the maximum value of the dynamic tire load remains almost the same.

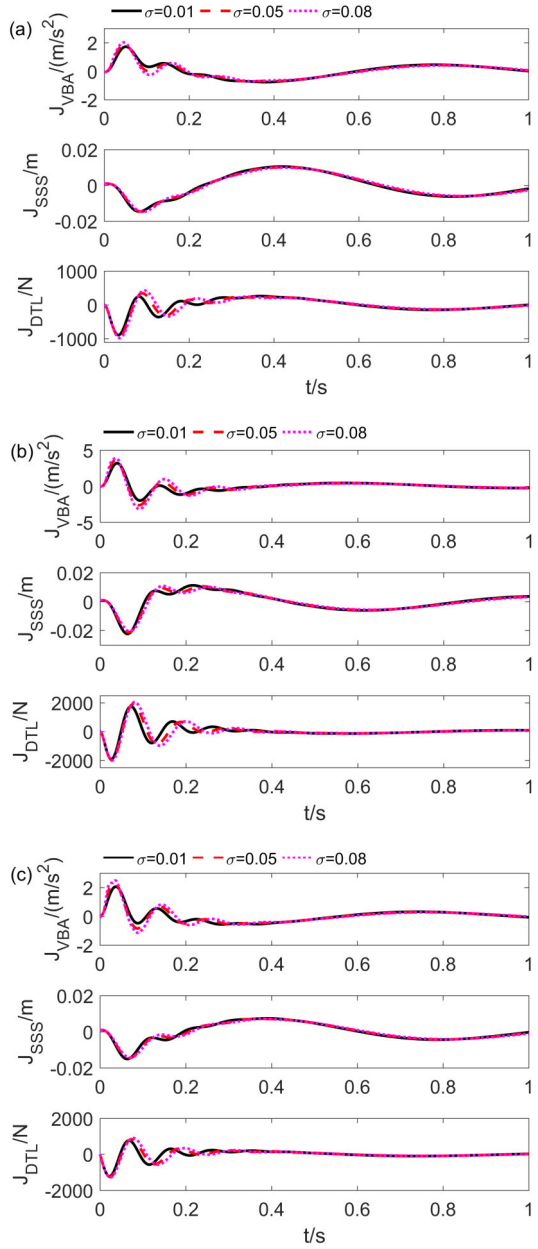

Fig. 18. Time history of three performance criteria for the TDA-IB suspension with different σ under shock excitation: (a) rounded step, (b) rounded pulse, and (c) oscillatory step ($\gamma = 5$, $\delta = 0.01$, $\tau = 0.01$ [s], $z_{r\max} = 0.02$ [m])

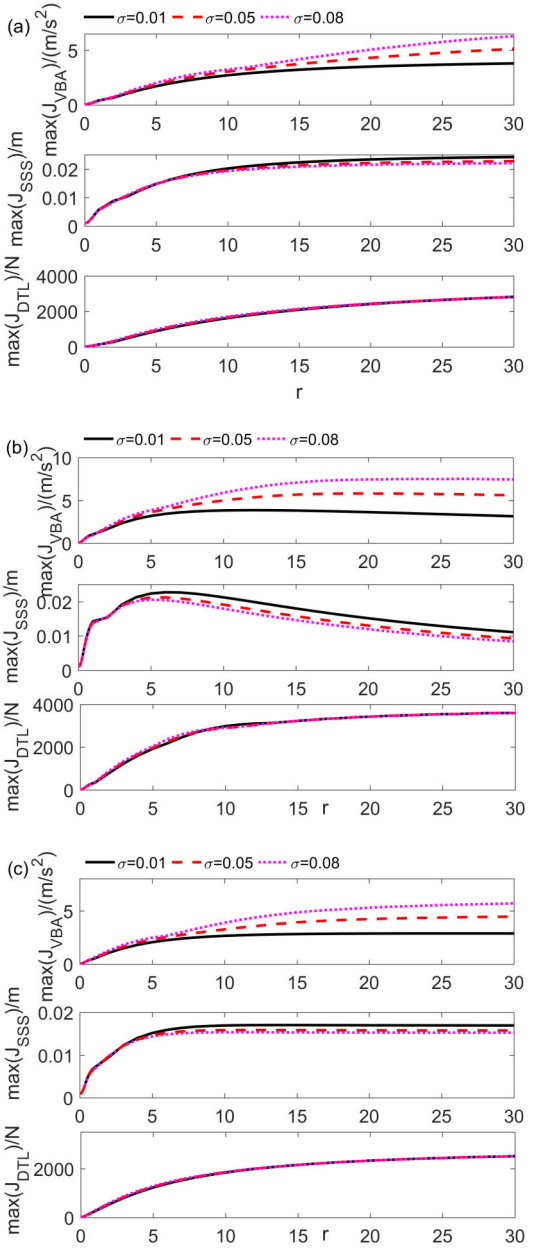

Fig. 19. The maximum values of three performance criteria for the TDA-IB suspension with different σ and γ: (a) rounded step, (b) rounded pulse, and (c) oscillatory step ($\delta = 0.01$, $\tau = 0.01$ [s], $z_{r\max} = 0.02$ [m])

5. CONCLUSIONS

This paper proposes an active inerter-based suspension with time-delayed acceleration feedback control. The stability analysis of the TDA-IB suspension is conducted using the definite integral stability method, the stable and unstable regions are determined. The effect of the time delay and feedback gain on the dynamic performance of the TDA-IB suspension under harmonic, random, and shock excitations is studied and compared with the PC-IB and traditional ones. The conclusions are summarized as follows:

- The dynamic equation of the TDA-IB suspension is an NDDE in which the time delay exists in the highest-order derivative, the stability could be analyzed conveniently by calculating the number of unstable characteristic roots based on the definite integral stability method, which is achieved by rounding off an integral of the characteristic function within a limited interval.
- The TDA-IB suspension is asymptotically stable for smaller feedback gain and time delay; through increasing the feedback gain, the stable regions shrink, and a smaller time delay could cause the system to be unstable.
- The time delay could regulate the resonance peak around the unsprung mass natural frequency and generate multiple high-frequency resonance peaks, if the time delay is chosen

appropriately and within the stable range, the TDA-IB suspension could improve the suspension stroke and dynamic tire load while having a degeneration for the vehicle body acceleration compared with the PC-IB and traditional suspensions.

Overall, the TDA-IB suspension is a novel design and could be utilized to improve the suspension stroke and dynamic tire load. In further work, the half-vehicle, full-vehicle, and more practical vehicle models equipped with TDA-IB suspension will be considered and the effect of the time delay and feedback gain on their dynamic performance will be conducted. Furthermore, experimental research will be carried out to verify the validity of the theoretical results.

APPENDIX

Abbreviation

CVT:	continuously variable transmission
NDDE:	neutral type of delay differential equation
PC:	parallel-connected
PC-IB:	parallel-connected inerter-based
PSD:	power spectral density
RDDE:	retarded type of delay differential equation
RMS:	root mean square
SA-IB:	semi-active inerter-based
TDA-IB:	time-delayed active inerter-based

ACKNOWLEDGEMENTS

This work was supported by the National Natural Science Foundation of China (Grant No. 12172153, 51805216, 51805217), State Key Laboratory of Mechanics and Control of Mechanical Structures (Nanjing University of Aeronautics and Astronautics (Grant No. MCMS-E-0220Y01), Key Laboratory of Road and Traffic Engineering of the Ministry of Education (Tongji University) (Grant No. K202005) and Vehicle Measurement, Control and Safety Key Laboratory of Sichuan Province (Grant No. QCCK2021-001).

REFERENCES

[1] R. Rajamani, *Vehicle Dynamics and Control*. New York, USA: Springer, 2012, doi: 10.1007/978-1-4614-1433-9.

[2] P. Baranowski and J. Malachowski, "Numerical study of selected military vehicle chassis subjected to blast loading in terms of tire strength improving," *Bull. Pol. Acad. Sci. Tech. Sci.*, vol. 63, no. 4, pp. 867–878, 2015, doi: 10.1515/bpasts-2015-0099.

[3] Y. Li, D.C. He, and Q.R. Si, "Theoretical and experimental analysis on the interaction properties between tracks and sediments considering sand content for unmanned underwater tracked bulldozer," *Bull. Pol. Acad. Sci. Tech. Sci.*, vol. 69, no. 1, e136036, 2021, doi: 10.24425/bpasts.2021.136036.

[4] M.C. Smith, "Synthesis of mechanical networks: the inerter," *IEEE Trans. Autom. Control.*, vol. 47, no. 10, pp. 1648–1662, 2002, doi: 10.1109/TAC.2002.803532.

[5] R.C. Wang, X.P. Meng, D.H. Shi, X.L. Zhang, Y.X. Chen, and L. Chen, "Design and test of vehicle suspension system with inerters," *Proc. Inst. Mech. Eng., Part C: J. Mech. Eng. Sci.*, vol. 228, no. 15, pp. 2684–2689, 2014, doi: 10.1177/0954406214521793.

[6] S.Y. Zhang *et al.*, "Ride comfort enhancement for passenger vehicles using the structure-immittance approach," *Veh. Syst. Dyn.*, 2019, doi: 10.1080/00423114.2019.1694158.

[7] X.F. Liu, J.Z. Jiang, A. Harrison, and X.X. Na, "Truck suspension incorporating inerters to minimise road damage," *Proc. Inst. Mech. Eng., Part D: J. Automob. Eng.*, vol. 234, no. 10-11, pp. 2693–2705, 2020, doi: 10.1177/ 0954407020905149.

[8] J.L. Yao, G.W. Lv, M. Qv, Z.H. Li, S. Ren, and S. Taheri, "Lateral stability control based on the roll moment distribution using a semiactive suspension," *Proc. Inst. Mech. Eng., Part D: J. Automob. Eng.*, vol. 231, no. 12, pp. 1627–1639, 2017, doi: 10.1177/0954407016681386.

[9] L. Yang, R.C. Wang, X.P. Meng, Z.Y. Sun, W. Liu, and Y. Wang, "Performance analysis of a new hydropneumatic inerter-based suspension system with semi-active control effect," *Proc. Inst. Mech. Eng., Part D: J. Automob. Eng.*, vol. 234, no. 7, pp. 1883–1896, 2020, doi: 10.1177/0954407019894189.

[10] M. Lazarek, P. Brzeski, and P. Perlikowski, "Design and identification of parameters of tuned mass damper with inerter which enables changes of inertance," *Mech. Mach. Theory*, vol. 119, pp. 161–173, 2018, doi: 10.1016/j.mechmachtheory.2017.09.004.

[11] M. Lazarek, P. Brzeski, and P. Perlikowski, "Design and modeling of the CVT for adjustable inerter," *J. Franklin Inst.*, vol. 356, pp. 7611–7625, 2019, doi: 10.1016/j.jfranklin.2018.11.011.

[12] R. Faraj, L. Jankowski, C. Graczykowski, and J. Holnicki-Szulc, "Can the inerter be a successful shock-absorber? The case of a ball-screw inerter with a variable thread lead," *J. Franklin Inst.*, vol. 356, pp. 7855–7872, 2019, doi: 10.1016/j.jfranklin.2019.04.012.

[13] M.Z.Q. Chen, Y.L. Hu, C.Y. Li, and G.R. Chen, "Application of semi-active inerter in semi-active suspensions via force tracking," *J. Vib. Acoust.*, vol. 138, no. 4, p. 041014, 2016, doi: 10.1115/ 1.4033357.

[14] X.L. Zhang, T. Zhang, J.M. Nie, and L. Chen, "A semiactive skyhook-inertance control strategy based on continuously adjustable inerter," *Shock Vib.*, vol. 2018, p. 6828621, 2018, doi: 10.1155/2018/6828621.

[15] X.J. Zhang, M. Ahmadian, and K.H. Guo, "On the benefits of semi-active suspensions with inerters," *Shock Vib.*, vol.19, no. 3, pp. 257–272, 2012, doi: 10.3233/SAV-2011-0628.

[16] Y.L. Hu, M.Z.Q. Chen, and Y. Sun, "Comfort-oriented vehicle suspension design with skyhook inerter configuration," *J. Sound Vib..*, vol. 405, pp. 34–47, 2017, doi: 10.1016/j.jsv.2017.05.036.

[17] Y. Wang, H. Ding, and L.Q. Chen, "Averaging analysis on a semi-active inerter-based suspension system with relative-acceleration- relative-velocity control," *J. Vib. Control*, vol. 26, no. 13–14, pp. 1199–1215, 2020, doi: 10.1177/1077546319 89 1612.

[18] W.C. Sun, H.H. Pan, Y.F. Zhang, and H. Gao, "Multi-objective control for uncertain nonlinear active suspension systems," *Mechatronics*, vol. 24, no. 4, pp. 318–327, 2014, doi: 10.1016/j.mechatronics.2013.09.009.

[19] Y.B. Huang, J. Na, X. Wu, X.Q. Liu, and Y. Guo, "Adaptive control of nonlinear uncertain active suspension systems with prescribed performance," *ISA Trans.*, vol. 54, pp. 145–155, 2015, doi: 10.1016/j.isatra.2014.05.025.

[20] H.N. He, Y. Li, J.Z. Jiang, S. Burrow, S.A. Neild and A. Conn, "Using an inerter to enhance an active-passive-combined vehicle suspension system," *Int. J. Mech. Sci.*, vol. 204, p. 106535, 2021, doi: 10.1016/j.ijmecsci.2021.106535.

[21] I.G. Jin and G. Orosz, "Dynamics of connected vehicle systems with delayed acceleration feedback," *Transport Res. C-Emer.*, vol. 46, pp. 46–64, 2014, doi: 10.1016/j.trc.2014.04.014.

[22] Q. Xu, G. Stepan and Z.H. Wang, "Balancing a wheeled inverted pendulum with a single accelerometer in the presence of time delay", *J. Vib. Control*, vol. 23, no. 4, pp. 604–614, 2017, doi: 10.1177/1077546315583400.

[23] Z.N. Masoud and A.H. Nayfeh, "Sway reduction on container cranes using delayed feedback controller," *Nonlinear Dyn.*, vol. 34, pp. 347–358, 2003, doi: 10.1023/B:NODY.0000013512.43841.55.

[24] Q. Xu and Z.H. Wang, "Exact stability test of neutral delay differential equations via a rough estimation of the testing integral," *Int. J. Dyn. Control*, vol. 2, no. 2, pp. 154–163, 2014, doi: 10.1007/s40435-013-0044-7.

[25] Y. Wang, S.M. Li, C. Cheng, and Y.Q. Su, "Adaptive control of a vehicle-seat-human coupled model using quasi-zero-stiffness vibration isolator as seat suspension," *J. Mech. Sci. Technol.*, vol. 32, no. 7, pp. 2973–2985, 2018, doi: 10.1007/s12206-018-0601-2.

[26] D. Ivanescu, S.I. Niculescu, L. Dugard, J.M. Dion, and E.I. Verriest, "On delay-dependent stability for linear neutral systems," *Automatica*, vol. 39, no. 2, pp. 255–261, 2003, doi: 10.1016/S0005-1098(02)00227-3.

[27] G.I.K. Taffo, M.S. Siewe, and C. Tchawoua, "Stability switches and bifurcation in a two-degrees-of-freedom nonlinear quarter-car with small time-delayed feedback control," *Chaos Solitons Fractals*, vol. 87, pp. 226–239, 2016, doi: 10.1016/j.chaos.2016.04.012.

[28] S. Rifat and N. Olgac, "Complete stability analysis of neutral-type first order two-time-delay systems with cross-talking delays," *SIAM J. Control Optim.*, vol. 45, no. 3, pp. 957–971, 2006, doi: 10.1137/050633810.

[29] T. Insperger, G. Stepan, and T. Janos, "Delayed feedback of sampled higher derivatives," *Philos. Trans. R. Soc. London, Ser. A*, vol. 368, no. 1911, pp. 469–482, 2010, doi: 10.1098/rsta.2009.0246.

[30] T. Vyhlidal, N. Olgac, and V. Kucera, "Delayed resonator with acceleration feedback-Complete stability analysis by spectral methods and vibration absorber design," *J. Sound Vib.*, vol. 333, no. 25, pp. 6781–6795, 2014, doi: 10.1016/j.jsv.2014.08.002.

[31] Q. Xu, G. Stepan, and Z.H. Wang, "Delay-dependent stability analysis of time-delay systems by using delay-independent evaluation," *Automatica*, vol. 70, pp. 153–157, 2016, doi: 10.1016/j.automatica.2016.03.028.

[32] G. Verros, S. Natsiavas, and C. Papadimitriou, "Design optimization of quarter-car models with passive and semi-active suspensions under random road excitation," *J. Vib. Control*, vol. 11, no. 5, pp. 581–606, 2005, doi: 10.1177/1077546305052315.

[33] M. Silveira, B.R. Pontes and J.M. Balthazar, "Use of nonlinear asymmetrical shock absorber to improve comfort on passenger vehicles," *J. Sound Vib.*, vol. 333, no. 7, pp. 2114–2129, 2014, doi: 10.1016/j.jsv.2013.12.001.